

# 2D Materials as Effective Cantilever Piezoelectric Nano Energy Harvesters

Yang Nan,<sup>||</sup> Dan Tan,<sup>||</sup> Jiajia Shao, Morten Willatzen,<sup>\*</sup> and Zhong Lin Wang<sup>\*</sup>Cite This: *ACS Energy Lett.* 2021, 6, 2313–2319

Read Online

ACCESS |



Metrics &amp; More

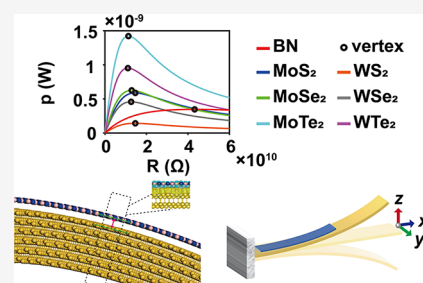


Article Recommendations



Supporting Information

**ABSTRACT:** Two-dimensional (2D) layered piezoelectric nanomaterials are attractive for application in mechanical energy-harvesting devices. In this study, layered 2D nanosheets, h-BN and  $\text{MX}_2$  ( $\text{M} = \text{Mo}$  or  $\text{W}$ ;  $\text{X} = \text{S}$ ,  $\text{Se}$ , or  $\text{Te}$ ), are deposited on a silicon substrate to form cantilever energy harvesters. Using density functional theory (DFT) and molecular dynamics (MD) calculations, the effect of the substrate for energy harvesting is studied. The substrate provides 2D layers with stable support while maintaining effective energy harvesting. MD results indicate that the electromechanical conversion energy has contributions from piezoelectricity and flexoelectricity, but the latter is negligible due to small strain gradients for bending-operated nanoharvesters. It is shown that the out-of-plane piezoelectric constants are substantially larger than their in-plane piezoelectric counterparts. The output power is calculated for a substrate-supported nanogenerator. This work provides an atomistic study of piezoelectricity and a new strategy to implement 2D materials in nano energy harvesters.



Piezoelectricity is an energy effective mechanism to establish mechanical and electrical dynamic control in nanodevices. Owing to its high transformation capability and response sensitivity, piezoelectricity is widely used in sensors,<sup>1–3</sup> transducers,<sup>4,5</sup> etc. Inspired by a milestone work contributed by Wang et al.<sup>6</sup> about piezoelectric nanogenerators based on zinc oxide (ZnO) nanowire arrays, researchers are focusing more attention on the study of piezoelectric materials at the nanoscale. Among these materials, 2D piezoelectric nanomaterials (PNMs) have many advantages over their bulk constituents. For example, 2D materials are more flexible and can sustain large strain. The ability to withstand high deformation extends the applications of devices working in complex and large strain environments like human activities.<sup>2</sup> In effect, the piezoelectric properties of PNMs can be dramatically modified. A main reason for this is that, increasing with downscaling, surfaces play a relatively larger role for material properties. Therefore, surface atom modifications can drastically modify properties of single-layered materials which are one atom or one molecular layer thick. While graphene is non-piezoelectric because of its centrosymmetry, surface modifications can make graphene-based structures piezoelectric.<sup>7</sup> In addition to transforming non-piezoelectric materials into piezoelectric media, surface atom modifications can also lead to enhancement of piezoelectric coefficients of piezoelectric structures.<sup>8</sup> Despite their numerous advantages, the synthesis of 2D PNM smart structures is difficult to control in a way that avoids introducing unwanted vacancies or impurities. Furthermore, the light weight and small thickness

limit the applications of suspended 2D PNMs due to their mechanical fragility. In order to overcome these restrictions so as to utilize 2D PNMs, mechanical support through the substrate is important.

Most of the syntheses and applications of 2D materials are carried out on substrates. There are many advantages in synthesizing 2D materials on substrates, as this ensures high quality, large scale, and few defects. For example, the first successful attempt in realizing freestanding graphene was accomplished by mechanical exfoliation.<sup>9</sup> Despite excellent quality samples, the method suffers from poor scalability. In contrast, Hwang et al.<sup>10</sup> proposed a method to grow high-quality graphene through van der Waals epitaxy on a *c*-plane sapphire substrate. The presence of the substrate ensures stability and good quality during epitaxy of graphene. Further, substrates provide mechanical support for 2D materials to perform strain, vibration, bending, and other operations on a macroscale. Baek et al.<sup>11</sup> synthesized  $\text{Pb}(\text{Mg}_{1/3}\text{Nb}_{2/3})\text{O}_3$ - $\text{PbTiO}_3$  (PMN-PT) thin films on vicinal (001) silicon and incorporated these heterostructures into microcantilevers to harvest energy. The Si substrate enables structures with precisely specified passive-layer thicknesses to control stiffness

Received: April 30, 2021

Accepted: May 24, 2021

and displacement. The strain induced in the 2D materials can be precisely and homogeneously controlled by the substrate. Zeng et al.<sup>12</sup> developed a spherical diameter engineering process to tune the bandgap of monolayer MoS<sub>2</sub>. Furthermore, the precise control of strain is important for energy harvesting. Wu et al.<sup>13</sup> used a polyethylene terephthalate (PET) flexible substrate to control the strain of monolayer MoS<sub>2</sub> to generate piezoelectric voltages and then form a nanogenerator to harvest energy. Different from the piezoelectric voltage generated along the armchair direction, Kim et al.<sup>14</sup> put forward an electrical output along the armchair and zigzag directions of a triangular-shaped MoS<sub>2</sub> monolayer. The output power of a nanogenerator based on movement along the armchair direction is twice as large compared to that along the zigzag direction. The synthesis process and nanogenerator operations are all carried out on a substrate. In contrast to the pioneering studies on piezoelectricity in materials containing an odd number of layers, Lee et al.<sup>15</sup> verified that a piezoelectric response can be found in bilayer WSe<sub>2</sub> through turbostratic stacking. In their study, monolayered WSe<sub>2</sub> is first synthesized on a sapphire substrate and then transferred to a flexible PET substrate. On this basis, another monolayered WSe<sub>2</sub> is synthesized and transformed onto the former monolayered WSe<sub>2</sub> to form a turbostratic stacking structure. The turbostratic stacking bilayer WSe<sub>2</sub> retains the piezoelectric effect and is tested with high output power. Lee et al.<sup>4</sup> used a mechanochemical exfoliation method to obtain 2D piezoelectric hexagonal boron nitride (h-BN) nanoflakes and transfer them onto an electrode line-patterned plastic substrate to characterize their ability for harvesting energy. The utilization of a substrate allows precise characterization of energy generation from 2D piezoelectric BN nanoflakes. Recently, Kuang et al.<sup>16</sup> incorporated BN nanosheets of a few percent in weight ratio into polydimethylsiloxane (PDMS) to form composites. With the support of PDMS, BN nanosheets are able to produce piezoelectric voltages up to ~5.4 V with  $d_{33} \approx 12$  pC/N. Besides, lead(II) iodide (PbI<sub>2</sub>) nanosheets<sup>17</sup> and  $\alpha$ -In<sub>2</sub>Se<sub>3</sub><sup>18</sup> are used simultaneously with substrates to construct flexible 2D piezoelectric devices to harvest energy.

In this study, several 2D PNMs are deposited on a Si (111) surface to form cantilever beams to study the substrate effect on energy harvesting of 2D PNMs using density functional theory (DFT) and molecular dynamics (MD) methods. The DFT method has been widely used as an accurate approach to describe electronic structures of crystals as well as charge distributions in energy-harvesting devices like piezoelectric and triboelectric nanogenerators. The DFT results here allow determining charge differences between the substrate and 2D PNMs. To limit the combined computational efforts, we determine the separation of the substrate and the 2D PNMs during bending using MD instead of DFT. Then, by combining the DFT and MD results, the effects of the substrate on the application of 2D PNMs are obtained and discussed. MD results allow us to determine the polarization change and the piezoelectric characteristics of the 2D PNMs. The differences between bent and corrugated structures are also discussed. After that, a cantilever beam model using 2D PNMs is proposed as an energy-harvesting structure.

Formal Si has a diamond structure with lattice constant parameters of  $a = b = c = 5.4$  Å (shown in Figure 1a), while the lattice constants are  $a = b = 3.8$  Å (Figure 1b) when Si is cut to expose the (111) surface. Because the hexagonal close-packed

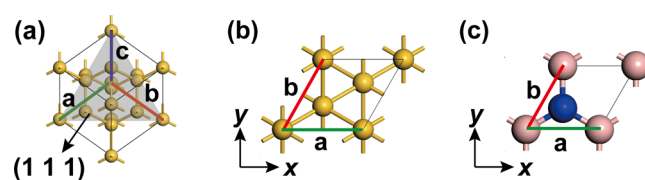


**Figure 1.** Atomic structures for (a) bulk Si, (b) Si (111), and (c) h-BN. Distances  $a$ ,  $b$ , and  $c$  for the three structures are shown in the respective plots.

2D layers have the same configuration, we only give the sketch of h-BN (Figure 1c). The details of heterostructures of BN and MX<sub>2</sub> with Si (111) and simulations of DFT and MD can be found in the Supporting Information.

As mentioned earlier, substrates are important for the synthesis and application of 2D PNMs with elastic and transparent features. However, the effects of the substrate on 2D PNMs' properties are not well known. The substrate is essential to maintain a robust and sustainable device. Further, it is evident from eq S14 that the induction of charges by the substrate is important to determine the polarization. Before studying the charge transfer at the interface, we first optimize the heterostructures listed in Table S1. The side views of the optimized heterostructures are shown in Figure S2. Table S4 gives the obtained equilibrium distance between the 2D PNMs and the Si substrate. A Bader charge analysis<sup>19</sup> is carried out to quantify the amounts of transferred charge for each heterostructure, and the calculated values of transferred charges for each unit cell are tabulated in Table S5. In order to analyze the charge transfer quantitatively, the amount of transferred charge  $\delta$ , defined as  $\delta = (\eta_c/\eta_{tot}) \times 100\%$ , is determined where  $\eta_c$  is the transferred charge and  $\eta_{tot}$  is the total charge for an isolated 2D layer. The calculated values are listed in Table S5. Our DFT calculations reveal that the charge transfer between the 2D layers and the Si (111) surface is small. Thus, the transferred charges do not affect the piezoelectric properties of heterostructures in MD.

We have carried out calculations of charge transfer under ideal conditions where the total energy, force, and distance between Si and 2D PNMs are in equilibrium. It has been confirmed that the maximum amount of charge transfer is localized at the equilibrium separation based on the overlapped electron-cloud theory.<sup>20</sup> Hence, the amount of transferred charges reaches a maximum at the equilibrium distance. However, conditions in actual applications can be such that the separation between the material and the substrate changes in time. To better understand this situation, a bent BN with Si as substrate is modeled in the MD simulations to evaluate the charge transfer. The simulations reveal that the separation of the bent BN 2D layer and the Si substrate is constant during a dynamic bending situation. A local intersurface is parallel because of the small strain gradient. The dashed area in Figure S3 is analyzed in a DFT calculation, and the charge density difference is shown in the inset. Bader charge analysis shows that the transferred charge of the bending configuration for each cell which contains 7 B–N pairs is 0.028 e, i.e., substantially smaller than the 0.497 e of the initial configuration. Hence, the effect of the transferred charge on the value of the piezoelectric coefficient can be neglected. This conclusion gives strong evidence of the stability of 2D materials subject to bending, and the only role of the substrate is to provide stability and strain.

The piezoelectric tensor depends strongly on the macroscopic shape.<sup>21</sup> The bent rectangular-shaped monolayers BN and MX<sub>2</sub> belong to the *monoclinic m* point group.<sup>22</sup> For the *monoclinic m* class, the piezoelectric matrix is

$$\mathbf{e} = \begin{pmatrix} e_{xxx} & e_{xyy} & e_{xzz} & 0 & e_{xxz} & 0 \\ 0 & 0 & 0 & e_{yyz} & 0 & e_{yxy} \\ e_{zxx} & e_{zyy} & e_{zzz} & 0 & e_{zxx} & 0 \end{pmatrix} \quad (1)$$

The polarization tensor and strain tensor take the forms

$$\mathbf{P} = \begin{pmatrix} P_1 \\ P_2 \\ P_3 \end{pmatrix}, \quad \mathbf{S} = \begin{pmatrix} S_{xx} \\ S_{yy} \\ S_{zz} \\ S_{yz} \\ S_{xz} \\ S_{xy} \end{pmatrix} \quad (2)$$

Figure 2 shows a bending configuration of BN. The curvature radius is 320 Å, and the strain and strain gradient curves are

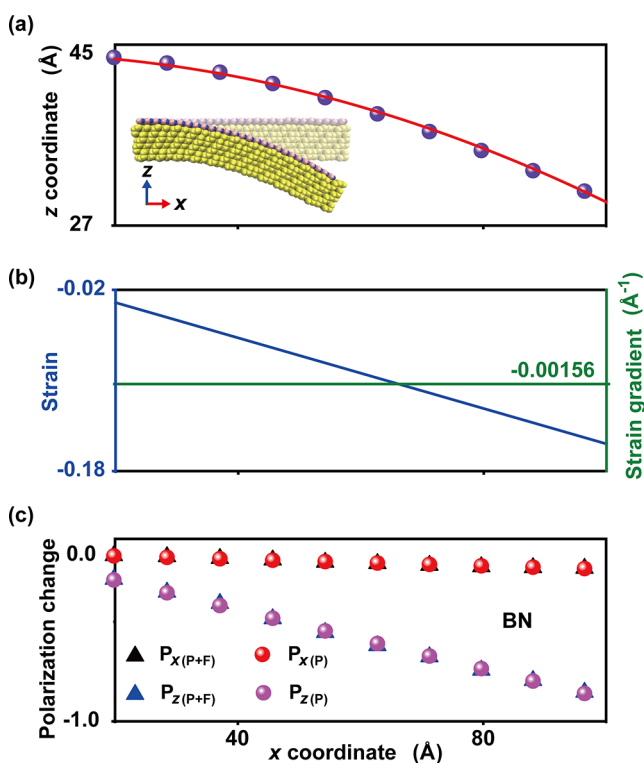


Figure 2. (a) Fitting curve of a bending configuration with a 320 Å curvature radius, (b) the strain and the strain gradient curves, and (c) polarization change due to piezoelectricity and flexoelectricity for 2D BN on a Si substrate.

obtained by fitting the displacement equation shown in Figure 2b. In our case, the bending displacement can be fitted as

$$u_z(x) = \alpha x^2 + \beta b \quad (3)$$

where  $\alpha$  and  $\beta$  are fitting parameters obtained from MD simulation. Since the displacements are along the  $z$  direction, the only non-zero strain component we have is  $S_{xz} = \frac{\partial u_z(x)}{\partial x}$ .

The relationship between  $\alpha$  and curvature radius  $r$  is  $\frac{1}{r} =$

$$\left| \frac{\partial^2 u_z(x)}{\partial x^2} \right| = |2\alpha|. \quad \text{According to } \mathbf{P} = \mathbf{e} \cdot \mathbf{S}, \text{ we have}$$

$$P_x = e_{xxz} S_{xz} \quad (4)$$

$$P_z = e_{zxx} S_{xz} \quad (5)$$

The polarization contains both piezoelectric and flexoelectric contributions when the structure is bent. The polarization in this bending configuration can be expressed as

$$P_x = e_{xxz} S_{xz} + \mu_{xxzx} \frac{\partial S_{xz}}{\partial x} \quad (6)$$

$$P_z = e_{zxx} S_{xz} + \mu_{zxxz} \frac{\partial S_{xz}}{\partial x} \quad (7)$$

where  $P_x$  and  $P_z$  are the polarization components along the  $x$  and  $z$  directions, respectively,  $e$  is the piezoelectric constant, and  $\mu$  denotes the flexoelectric constant. We note again that the only non-zero strain and strain-gradient components are  $S_{xz}$  and  $\delta S_{xz}/\delta x$ , respectively. The polarization change along the  $z$  direction indicates the out-of-plane piezoelectric response in 2D materials, which has been experimentally observed.<sup>23,24</sup> In this study, the displacement  $u_z(x)$  of each bending structure is fitted first. Then, eqs 6 and 7 are used to obtain the piezoelectric and flexoelectric constants from MD calculations.

Figure 2c shows the polarization changes along the  $x$  and  $z$  directions of BN for a bending configuration.  $P_{x(P+F)}$  ( $P_{z(P+F)}$ ) represents the total polarization change along the  $x$  ( $z$ ) direction, which has contributions from both piezoelectricity and flexoelectricity.  $P_{x(P)}$  ( $P_{z(P)}$ ) is the polarization change due to piezoelectricity alone. Our results show that both polarization components have their main contribution from the piezoelectric effect and the flexoelectric contribution is negligible. Similar conclusions are obtained for MX<sub>2</sub>. As shown in Figure S4, the results agree well with those in ref 22.

The macroscopic shape and the boundary conditions of 2D materials are essential in determining the piezoelectric properties. A systematic analysis of the difference between the bending and corrugated configurations is performed for better understanding the importance of symmetry (Supporting Information). Then, several bending configurations are calculated to obtain the dependency of polarization change and bending curvature. For each 2D layer, the polarization changes of five configurations during the bending process are calculated. The results of BN and MoS<sub>2</sub> are shown in Figure 3, where  $a_i$  ( $i = 1, 2, 3$ ) represents BN,  $b_i$  ( $i = 1, 2, 3$ ) are MoS<sub>2</sub>, subscripts 1 and 2 are the polarization change along the  $x$ - and  $z$ -direction, respectively, while subscript 3 represents the relationship between the bending curvature and the polarization change. The analyses of bending configurations of other MX<sub>2</sub> are shown in Figure S5. Apparently, polarization changes are linearly related to bending curvature. In addition, the piezoelectric constant can be obtained by solving eqs 4 and 5, where we have

$$e_{xxz} = \frac{P_x}{S_{xz}} = \frac{k_x x}{\frac{r}{2ax}} = k_x \quad (8)$$

$$e_{zxx} = \frac{P_z}{S_{xz}} = \frac{k_z x}{\frac{r}{2ax}} = k_z \quad (9)$$

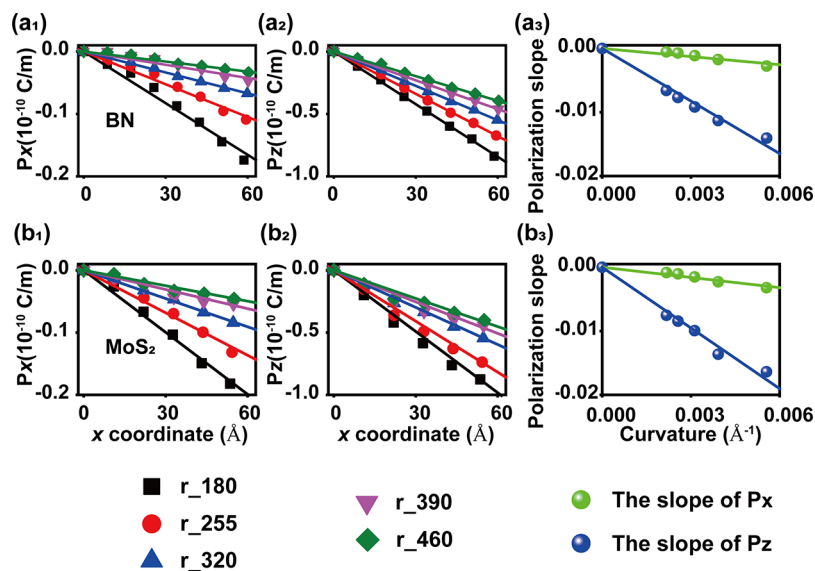


Figure 3. Polarization changes for different bending configurations of (a) BN and (b) MoS<sub>2</sub>, where the left and middle columns represent polarization changes along the *x*- and *z*-axis, respectively, while the right column shows the polarization changes vs curvature.

Here,  $k_x$  and  $k_z$  are the slopes calculated in the third column figures in Figure 3. For our bending models, the calculated piezoelectric constants are tabulated in Table 1. One interesting thing is that the trends of piezoelectric constants  $e_{xxz}$  and  $e_{zxx}$  of MX<sub>2</sub> are the same as that of piezoelectric constant  $e_{xxx}$  reported by Blonsky et al.<sup>25</sup>

Table 1. Piezoelectric Constants of Different Materials (10<sup>-10</sup> C/m)

	$e_{xxz}$	$e_{zxx}$
BN	-0.42	-2.75
MoS <sub>2</sub>	-0.53	-3.17
MoSe <sub>2</sub>	-0.94	-3.62
MoTe <sub>2</sub>	-1.27	-6.32
WS <sub>2</sub>	-0.26	-1.56
WSe <sub>2</sub>	-0.46	-3.15
WTe <sub>2</sub>	-1.13	-5.23

After we determine the relationship between bending and the polarization change, a cantilever-like piezoelectric nanogenerator composed of 2D material is designed to harvest mechanical energy, as shown in Figure 4a. The free charge

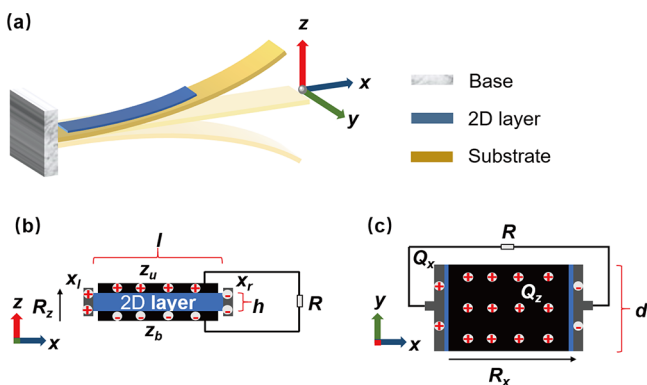


Figure 4. Schematic showing (a) a nanogenerator and charge distribution, (b) side view, and (c) top view.

distribution and the hooked-up external load resistance are shown in Figure 4b,c. It has been confirmed by MD results that the polarization  $P(x)$  (along *x* and *z* directions) is a function of the only strain component present,  $S_{xz}(x)$ . The time-dependent polarization for an angular frequency  $\omega$  has the format

$$P(x, t) = P(x) \exp(i\omega t) \quad (10)$$

Here,  $P(x)$  is the polarization change for bulk materials.

For a nanogenerator operation, according to Maxwell's equations, the electric displacement vector is

$$D = \epsilon E + P_{\text{piezo}} \quad (11)$$

where  $E$  is the electric field,  $P_{\text{piezo}}$  is the polarization created by mechanical vibration, and  $\epsilon$  is the permittivity of the dielectric. The permittivity in this study is divided into the in-plane and out-of-plane values, which are  $\epsilon_{\parallel}$  and  $\epsilon_{\perp}$ , respectively.

The total output in our model is generated by (details shown in Supporting Information)

$$p_{\text{tot}} = \frac{1}{T} \int_0^T [p_x(t) + p_z(t)] dt = \frac{\omega^2 A_1^2 l^4 \epsilon_{xxz}^2 R}{8h^2 r^2 (\omega^2 R_1^2 A_1^2 \epsilon_{\parallel}^2 + l^2)} + \frac{\omega^2 A_3^2 l^2 \epsilon_{zxx}^2 R}{8r^2 (\omega^2 R_3^2 A_3^2 \epsilon_{\perp}^2 + h^2)} \quad (12)$$

where  $T$  indicates the vibration period, that is,  $T = 2\pi/\omega$ .

In this study, the power output generated by cantilever-like piezoelectric nanogenerators can be calculated by implementing the above expressions. Figure 5a shows the total output power generated detected by a BN nanosheet with dimensions  $l = 10 \mu\text{m}$  and  $d = 5 \mu\text{m}$ . The output power increases at first and then decreases when the external resistance reaches optimum. The power output has the same tendency as the experimental result but gives somewhat larger values.<sup>13</sup> We note that the proposed bending model has polarization changes along two different directions; hence, both the contributions of output power  $p_x$  and  $p_z$  are analyzed. It is shown in Figure 5b that  $p_{\text{tot}}$  is mainly due to  $p_z$  for relatively small resistances. As the resistance increases,  $p_x$  eventually reaches its optimum output, which can be seen in the inset of

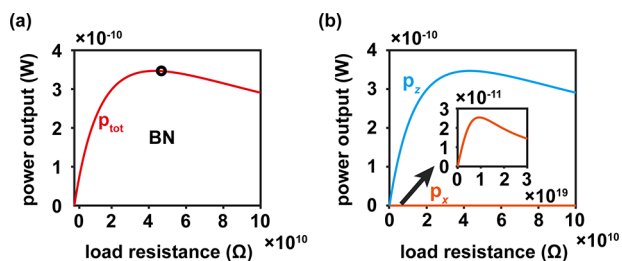


Figure 5. Dependence of the output power on the external load resistance (2D BN): (a)  $p_{\text{tot}}$  and (b)  $p_x$  and  $p_z$ . The inset shows  $p_x$  vs the corresponding load resistance.

Figure 5b. However, as the external resistance in practice cannot increase to the high values required at optimum, we only consider the output due to  $p_z$ .

The relationship between output power and external resistance of BN and  $\text{MX}_2$  is shown in Figure 6a. The

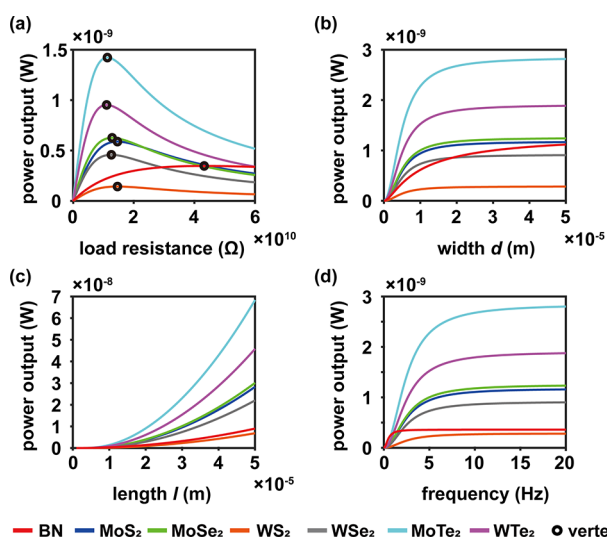


Figure 6. Dependence of the output power on (a) the external load resistance, (b) the width, (c) the length, and (d) the frequency of 2D BN and  $\text{MX}_2$ .

optimum resistance of each material is marked in the figure, and the values are tabulated in Table S6. The results show that  $\text{MoTe}_2$  (in comparison with other materials) has the highest output power at its optimum resistance. The trend of the maximum output power and the corresponding optimum resistance of  $\text{MX}_2$  are the same as for the piezoelectric constants as shown in Table 1, where  $\text{MTe}_2 > \text{MSe}_2 > \text{MS}_2$  and  $\text{MoX}_2 > \text{WX}_2$ . The same tendency indicates that the piezoelectric constant is the main factor that influences the output of the nanogenerators. Note that the output power of BN vs resistance follows the trend of the piezoelectric constant, but the position of the optimum resistance is different. The main reason is that, compared to  $\text{MX}_2$ , the electrical conductivity  $\kappa$  of BN is very small, which means the internal resistance of BN is correspondingly large. In addition to accounting for the disparity of optimum resistances between BN and  $\text{MX}_2$ , this large internal resistance affects the dependency of the output power on the width of 2D layers. Figure 6b reveals that the output of  $\text{MX}_2$  first increases and then becomes constant after the width reaches 0.2 mm, as the width is the only variable. Since the output power of BN is

significantly smaller compared to other materials, BN needs a larger width to reach its constant output power. The dependency of output on the length is shown in Figure 6c. The output power is a quadratic function of the side length of the 2D layers, and the arrangement of the output power is related to the piezoelectric constants. Figure 6d shows that the output powers of all materials detected in this study are increasing at first and then nearly unchanged when the frequency is increased to 10 Hz, which shows a similar tendency as the comparison of a piezoelectric nanogenerator and a triboelectric nanogenerator.<sup>26</sup> Among these 2D layers, BN rapidly reaches a constant output power because of its large internal resistance.

Here we propose a stable, simple piezoelectric nanogenerator prototype with an output power in the range of  $(1.42\text{--}14.2) \times 10^{-10}$  W (Table S6). With the support of the substrate, the 2D PNMs examined are good candidates for energy harvesting with a high total output. Our results show that, for load resistance values below 1 teraohm, only the out-of-plane piezoelectric polarization component contributes significantly to energy harvesting. Observe that the discrepancy in optimal load resistances  $R_1$  and  $R_3$  is a consequence of the generator length being much larger than the generator thickness (Figure S6). In comparison, the experimental output power reported by Wang et al.<sup>13</sup> is  $5.53 \times 10^{-14}$  W at the load resistance optimum. Han et al.<sup>27</sup> summarized a range of output powers of most piezoelectric nanogenerators as  $(0.005\text{--}5) \times 10^{-11}$  W. These previously reported works are based solely on the out-of-plane piezoelectric polarization contribution, and usually the two ends of the device are fixed. A BN nanoribbon was reported by López-Suárez et al.<sup>28</sup> as an energy harvester that can reach an output of  $8 \times 10^{-12}$  W if the nanoribbon is pre-strained, which, however, is harder to control. The output of the graphene-like ZnO nanogenerator that we reported earlier is  $2.11 \times 10^{-11}$  W.<sup>22</sup> The cantilever nanogenerator structure that we study here is simpler, as only one side is fixed. In addition, this model is very flexible and provides several options for the choice of substrate and piezoelectric layers. Higher output power can be reached by considering materials with higher out-of-plane piezoelectric properties, like  $\text{SnS}^{29}$  and ZnO,<sup>30</sup> with specific thicknesses which have been studied experimentally. We anticipate that experimental work on this cantilever nanogenerator design is necessary to better justify the highest output power attainable. Our work provides a solid strategy for the use of 2D materials, such as BN and  $\text{MX}_2$ , for practical applications.

In summary, we have calculated the in-plane and out-of-plane piezoelectric properties of 2D layered PNMs and studied their application in energy harvesting. MD and DFT methods are combined first to study the substrate effect for energy harvesting. Different from the case with corrugated configurations, the charge transfer during the bending process is too weak to influence the piezoelectric properties of 2D layer. Furthermore, our MD results show that the polarization change has contributions from both piezoelectricity and flexoelectricity, but the latter can be ignored for bending configurations. A symmetry discussion related to graphene and  $\text{MoX}_2$  for piezoelectric effects in bending configurations vs corrugation configurations is presented. Lastly, we consider energy-harvesting operation based on a cantilever nanogenerator structure and determine the output power calculated from Maxwell's displacement current generated by the mechanical motion.

## ■ ASSOCIATED CONTENT

### Supporting Information

The Supporting Information is available free of charge at <https://pubs.acs.org/doi/10.1021/acsenerylett.1c00901>.

Computational simulations details, symmetry discussion of bending and corrugated configurations, and theory of the output of piezoelectric nanogenerators, including Figures S1–S6, Tables S1–S6, and eqs S1–S33 (PDF)

## ■ AUTHOR INFORMATION

### Corresponding Authors

**Morten Willatzen** – CAS Center for Excellence in Nanoscience, Beijing Key Laboratory of Micro-nano Energy and Sensor, Beijing Institute of Nanoenergy and Nanosystems, Chinese Academy of Sciences, Beijing 100083, China; College of Nanoscience and Technology, University of Chinese Academy of Sciences, Beijing 100049, People's Republic of China; [orcid.org/0000-0002-8215-9650](https://orcid.org/0000-0002-8215-9650); Email: [mortenwillatzen@binn.cas.cn](mailto:mortenwillatzen@binn.cas.cn)

**Zhong Lin Wang** – CAS Center for Excellence in Nanoscience, Beijing Key Laboratory of Micro-nano Energy and Sensor, Beijing Institute of Nanoenergy and Nanosystems, Chinese Academy of Sciences, Beijing 100083, China; College of Nanoscience and Technology, University of Chinese Academy of Sciences, Beijing 100049, People's Republic of China; School of Materials Science and Engineering, Georgia Institute of Technology, Atlanta, Georgia 30332-0245, United States; [orcid.org/0000-0002-5530-0380](https://orcid.org/0000-0002-5530-0380); Email: [zhong.wang@mse.gatech.edu](mailto:zhong.wang@mse.gatech.edu)

### Authors

**Yang Nan** – CAS Center for Excellence in Nanoscience, Beijing Key Laboratory of Micro-nano Energy and Sensor, Beijing Institute of Nanoenergy and Nanosystems, Chinese Academy of Sciences, Beijing 100083, China; College of Nanoscience and Technology, University of Chinese Academy of Sciences, Beijing 100049, People's Republic of China; [orcid.org/0000-0002-2504-2982](https://orcid.org/0000-0002-2504-2982)

**Dan Tan** – CAS Center for Excellence in Nanoscience, Beijing Key Laboratory of Micro-nano Energy and Sensor, Beijing Institute of Nanoenergy and Nanosystems, Chinese Academy of Sciences, Beijing 100083, China; College of Nanoscience and Technology, University of Chinese Academy of Sciences, Beijing 100049, People's Republic of China

**Jiajia Shao** – CAS Center for Excellence in Nanoscience, Beijing Key Laboratory of Micro-nano Energy and Sensor, Beijing Institute of Nanoenergy and Nanosystems, Chinese Academy of Sciences, Beijing 100083, China; College of Nanoscience and Technology, University of Chinese Academy of Sciences, Beijing 100049, People's Republic of China

Complete contact information is available at: <https://pubs.acs.org/doi/10.1021/acsenerylett.1c00901>

### Author Contributions

<sup>†</sup>Y.N. and D.T. contributed equally to this work.

### Notes

The authors declare no competing financial interest.

## ■ ACKNOWLEDGMENTS

This research is supported by the National Key R & D Project from Minister of Science and Technology (Grant No. 2016YFA0202704), National Natural Science Foundation of

China (Grant Nos. 12002054 and 62001031), China Postdoctoral Science Foundation (Grant No. 2019M660766), and Fundamental Research Funds for the Central Universities (Grant No. E0E48957).

## ■ REFERENCES

- (1) Dai, M.; Wang, Z.; Wang, F.; Qiu, Y.; Zhang, J.; Xu, C. Y.; Zhai, T.; Cao, W.; Fu, Y.; Jia, D.; Zhou, Y.; Hu, P. A. Two-Dimensional van der Waals Materials with Aligned In-Plane Polarization and Large Piezoelectric Effect for Self-Powered Piezoelectric Sensors. *Nano Lett.* **2019**, *19*, 5410.
- (2) Kim, K.-B.; Jang, W.; Cho, J. Y.; Woo, S. B.; Jeon, D. H.; Ahn, J. H.; Hong, S. D.; Koo, H. Y.; Sung, T. H. Transparent and flexible piezoelectric sensor for detecting human movement with a boron nitride nanosheet (BNNS). *Nano Energy* **2018**, *54*, 91.
- (3) Khan, U.; Hinchet, R.; Ryu, H.; Kim, S.-W. Research Update: Nanogenerators for self-powered autonomous wireless sensors. *APL Mater.* **2017**, *5*, 073803.
- (4) Lee, G. J.; Lee, M. K.; Park, J. J.; Hyeon, D. Y.; Jeong, C. K.; Park, K. I. Piezoelectric Energy Harvesting from Two-Dimensional Boron Nitride Nanoflakes. *ACS Appl. Mater. Interfaces* **2019**, *11*, 37920.
- (5) Falconi, C. Piezoelectric nanotransducers. *Nano Energy* **2019**, *59*, 730.
- (6) Wang, Z. L.; Song, J. Piezoelectric Nanogenerators Based on Zinc Oxide Nanowire Arrays. *Science* **2006**, *312*, 242.
- (7) Ong, M. T.; Duerloo, K. A. N.; Reed, E. J. The Effect of Hydrogen and Fluorine Coadsorption on the Piezoelectric Properties of Graphene. *J. Phys. Chem. C* **2013**, *117*, 3615.
- (8) Noor-A-alam, M.; Kim, H. J.; Shin, Y. H. Dipolar polarization and piezoelectricity of a hexagonal boron nitride sheet decorated with hydrogen and fluorine. *Phys. Chem. Chem. Phys.* **2014**, *16*, 6575.
- (9) Novoselov, K. S.; Geim, A. K.; Morozov, S. V.; Jiang, D.; Zhang, Y.; Dubonos, S. V.; Grigorieva, I. V.; Firsov, A. A. Electric field effect in atomically thin carbon films. *Science* **2004**, *306*, 666.
- (10) Hwang, J.; Kim, M.; Campbell, D.; Alsalm, H. A.; Kwak, J. Y.; Shivaraman, S.; Woll, A. R.; Singh, A. K.; Hennig, R. G.; Gorantla, S.; Rummeli, M. H.; Spencer, M. G. van der Waals Epitaxial Growth of Graphene on Sapphire by Chemical Vapor Deposition without a Metal Catalyst. *ACS Nano* **2013**, *7*, 385.
- (11) Baek, S. H.; Park, J.; Kim, D. M.; Aksyuk, V. A.; Das, R. R.; Bu, S. D.; Felker, D. A.; Lettieri, J.; Vaithyanathan, V.; Bharadwaja, S. S.; Bassiri-Gharb, N.; Chen, Y. B.; Sun, H. P.; Folkman, C. M.; Jang, H. W.; Kreft, D. J.; Streiffer, S. K.; Ramesh, R.; Pan, X. Q.; Trolier-McKinstry, S.; Schlom, D. G.; Rzhowski, M. S.; Blick, R. H.; Eom, C. B. Giant piezoelectricity on Si for hyperactive MEMS. *Science* **2011**, *334*, 958.
- (12) Zeng, M.; Liu, J.; Zhou, L.; Mendes, R. G.; Dong, Y.; Zhang, M. Y.; Cui, Z. H.; Cai, Z.; Zhang, Z.; Zhu, D.; Yang, T.; Li, X.; Wang, J.; Zhao, L.; Chen, G.; Jiang, H.; Rummeli, M. H.; Zhou, H.; Fu, L. Bandgap tuning of two-dimensional materials by sphere diameter engineering. *Nat. Mater.* **2020**, *19*, 528.
- (13) Wu, W.; Wang, L.; Li, Y.; Zhang, F.; Lin, L.; Niu, S.; Chenet, D.; Zhang, X.; Hao, Y.; Heinz, T. F.; Hone, J.; Wang, Z. L. Piezoelectricity of single-atomic-layer MoS<sub>2</sub> for energy conversion and piezotronics. *Nature* **2014**, *514*, 470.
- (14) Kim, S. K.; Bhatia, R.; Kim, T. H.; Seol, D.; Kim, J. H.; Kim, H.; Seung, W.; Kim, Y.; Lee, Y. H.; Kim, S. W. Directional dependent piezoelectric effect in CVD grown monolayer MoS<sub>2</sub> for flexible piezoelectric nanogenerators. *Nano Energy* **2016**, *22*, 483.
- (15) Lee, J. H.; Park, J. Y.; Cho, E. B.; Kim, T. Y.; Han, S. A.; Kim, T. H.; Liu, Y.; Kim, S. K.; Roh, C. J.; Yoon, H. J.; Ryu, H.; Seung, W.; Lee, J. S.; Lee, J.; Kim, S. W. Reliable Piezoelectricity in Bilayer WSe<sub>2</sub> for Piezoelectric Nanogenerators. *Adv. Mater.* **2017**, *29*, 1606667.
- (16) Kuang, H.; Li, Y.; Huang, S.; Shi, L.; Zhou, Z.; Gao, C.; Zeng, X.; Pandey, R.; Wang, X.; Dong, S.; Chen, X.; Yang, J.; Yang, H.; Luo, J. Piezoelectric boron nitride nanosheets for high performance energy harvesting devices. *Nano Energy* **2021**, *80*, 105561.

(17) Song, H.; Karakurt, I.; Wei, M.; Liu, N.; Chu, Y.; Zhong, J.; Lin, L. Lead iodide nanosheets for piezoelectric energy conversion and strain sensing. *Nano Energy* **2018**, *49*, 7.

(18) Xue, F.; Zhang, J.; Hu, W.; Hsu, W. T.; Han, A.; Leung, S. F.; Huang, J. K.; Wan, Y.; Liu, S.; Zhang, J.; He, J. H.; Chang, W. H.; Wang, Z. L.; Zhang, X.; Li, L. J. Multidirection Piezoelectricity in Mono- and Multilayered Hexagonal alpha-In<sub>2</sub>Se<sub>3</sub>. *ACS Nano* **2018**, *12*, 4976.

(19) Tang, W.; Sanville, E.; Henkelman, G. A grid-based Bader analysis algorithm without lattice bias. *J. Phys.: Condens. Matter* **2009**, *21*, 084204.

(20) Lin, S.; Xu, C.; Xu, L.; Wang, Z. L. The Overlapped Electron-Cloud Model for Electron Transfer in Contact Electrification. *Adv. Funct. Mater.* **2020**, *30*, 1909724.

(21) Nan, Y.; Tan, D.; Zhao, J. Q.; Willatzen, M.; Wang, Z. L. Shape- and size dependent piezoelectric properties of monolayer hexagonal boron nitride nanosheets. *Nanoscale Advances* **2020**, *2*, 470.

(22) Tan, D.; Willatzen, M.; Wang, Z. L. Out-of-Plane Polarization in Bent Graphene-Like Zinc Oxide and Nanogenerator Applications. *Adv. Funct. Mater.* **2020**, *30*, 1907885.

(23) Seol, D.; Kim, S.; Jang, W.-S.; Jin, Y.; Kang, S.; Kim, S.; Won, D.; Lee, C.; Kim, Y.-M.; Lee, J.; Yang, H.; Jeong, M. S.; Belianinov, A.; Tselev, A.; Somnath, S.; Smith, C. R.; Ovchinnikova, O. S.; Balke, N.; Kim, Y. Selective patterning of out-of-plane piezoelectricity in MoTe<sub>2</sub> via focused ion beam. *Nano Energy* **2021**, *79*, 105451.

(24) Seo, J.; Kim, Y.; Park, W. Y.; Son, J. Y.; Jeong, C. K.; Kim, H.; Kim, W.-H. Out-of-plane piezoresponse of monolayer MoS<sub>2</sub> on plastic substrates enabled by highly uniform and layer-controllable CVD. *Appl. Surf. Sci.* **2019**, *487*, 1356.

(25) Blonsky, M. N.; Zhuang, H. L.; Singh, A. K.; Hennig, R. G. Ab Initio Prediction of Piezoelectricity in Two-Dimensional Materials. *ACS Nano* **2015**, *9*, 9885.

(26) Ahmed, A.; Hassan, I.; Helal, A. S.; Sencadas, V.; Radhi, A.; Jeong, C. K.; El-Kady, M. F. Triboelectric Nanogenerator versus Piezoelectric Generator at Low Frequency (<4 Hz): A Quantitative Comparison. *iScience* **2020**, *23*, 101286.

(27) Han, S. A.; Lee, J.; Lin, J.; Kim, S.-W.; Kim, J. H. Piezo/triboelectric nanogenerators based on 2-dimensional layered structure materials. *Nano Energy* **2019**, *57*, 680.

(28) Lopez-Suarez, M.; Abadal, G.; Gammaitoni, L.; Rurali, R. Noise energy harvesting in buckled BN nanoribbons from molecular dynamics. *Nano Energy* **2015**, *15*, 329.

(29) Khan, H.; Mahmood, N.; Zavabeti, A.; Elbourne, A.; Rahman, M. A.; Zhang, B. Y.; Krishnamurthi, V.; Atkin, P.; Ghasemian, M. B.; Yang, J.; Zheng, G.; Ravindran, A. R.; Walia, S.; Wang, L.; Russo, S. P.; Daeneke, T.; Li, Y.; Kalantar-Zadeh, K. Liquid metal-based synthesis of high performance monolayer SnS piezoelectric nanogenerators. *Nat. Commun.* **2020**, *11*, 3449.

(30) Mahmood, N.; Khan, H.; Tran, K.; Kuppe, P.; Zavabeti, A.; Atkin, P.; Ghasemian, M. B.; Yang, J.; Xu, C.; Tawfik, S. A.; Spencer, M. J. S.; Ou, J. Z.; Khoshmanesh, K.; McConville, C. F.; Li, Y.; Kalantar-Zadeh, K. Maximum piezoelectricity in a few unit-cell thick planar ZnO – A liquid metal-based synthesis approach. *Mater. Today* **2021**, *44*, 69.